The Journal of Physical Chemistry Letters

Biophysical Chemistry, Biomolecules, and Biomaterials; Surfactants and Membranes

Anisotropic Epitaxial Behavior in Amorphous Phase Mediated Hydroxyapatite Crystallization Process: A New Understanding of Orientation Control

Biao Jin, Changyu Shao, Yanming Wang, Zhao Mu, Zhaoming Liu, and Ruikang Tang

J. Phys. Chem. Lett., **Just Accepted Manuscript** • DOI: 10.1021/acs.jpclett.9b03109 • Publication Date (Web): 21 Nov 2019

Anisotropic Epitaxial Behavior in Amorphous Phase Mediated Hydroxyapatite Crystallization Process: A New Understanding of Orientation Control

Biao Jin, † *Changyu Shao,* † *Yanming Wang,* ‡ *Zhao Mu,* † *Zhaoming Liu** † *and Ruikang Tang** †

†Department of Chemistry, ‡State Key Laboratory of Silicon Materials, School of Materials Science and Engineering, Zhejiang University, Hangzhou, Zhejiang 310027, China

‡Department of Materials Science and Engineering Massachusetts Institute of Technology 77 Massachusetts Avenue, Cambridge, MA 02139, USA

Corresponding Author

*oldliu@zju.edu.cn

*rtang@zju.edu.cn

TOC Graphic

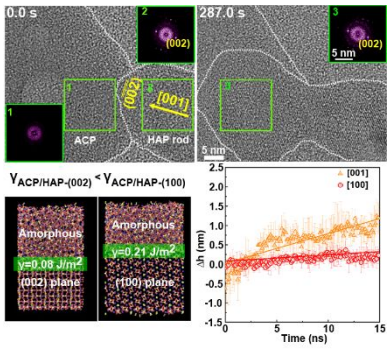

KEYWORDS: anisotropic crystallization, biomineralization, epitaxial growth, hydroxyapatite, phase transformation

ABSTRACT: The precise control of crystallization is a key in construction and engineering of crystalline materials, especially in biomineralization. Although it is generally accepted that biomineral crystals are evolved from their amorphous precursors, there are intensive debates about the crystallographic orientation control. By using in situ high resolution transmission electron microscopy (HR-TEM), we herein reveal that hydroxyapatite (HAP) produces through its epitaxial growth from amorphous calcium phosphate (ACP) with preferential *c-axis* orientation. Abnormally but interestingly, this anisotropic epitaxial crystallization priority along *c*-axis is not affected by the existed HAP crystalline substrate, which occurs exactly the same on either {002} or {100} facets. Molecular dynamic (MD) simulations suggest this preference is correlated with the interfacial energetic controls at the amorphous-crystalline transition frontier. The orientation control on biominerals here shows the key role of the interface energy, rather that the organic molecules or matrixes, which provides a complementary understanding about the general *c-axis* orientation control of HAP in various biomineralization case and develops an alternative strategy for crystallization control of functional materials.

Crystallographic orientation controls in crystal construction and engineering are of great importance to regulate physicochemical properties of materials for their functional applications.[1-8] In particular, the remarkable properties of minerals originate from their well-ordered and oriented hierarchical structures, which is attributed to their precise control over crystallization orientation.[9,10] Although classical crystal growth theory suggests that orientation control depends on selective adsorption and steric-hindrance effects of additives as well as organic matrix substrate,[11-14] it seems to be not applicable for biomineral crystals since amorphous precursor phase in crystallization process complicates the crystallization control.[15-17] It still keeps mysterious how these mineral crystals achieve orientation control through the transformation from amorphous to crystalline state.[18-22] For example, hydroxyapatite (HAP, Hexagonal with $P6_3/m$ space group symmetry),[23] a primary mineral phase in biological hard tissues (e.g. bone and dental enamel), always grows along *c-axis*.[24-26] Previous literatures show that inorganic ions, [27] biomolecules,[28,29] and even surfactants[30,31] can regulate the *c*-axis oriented growth of HAP. Although the adsorption effects of various additives on HAP surface are different, the explanations on crystalline orientation evolution regulated by these items are exactly the same. Thereby, there are intensive debates about the crystallographic orientation controls in biomineralization. It should be noted that continuous amorphous calcium phosphate (ACP) layer is often found at the crystallization front of HAP.[19] Notably and strangely, despite that the various crystal facets of HAP can be coated by ACP,[32] *c*-axis oriented crystallization is only documented in these biomineralization processes in nature, which follows a foundation of producing highly ordered multi-levels structures.[33] Moreover, such amorphous phase transformation mediated crystallization is distinguished from traditional epitaxial growth,[34-38] and the exact mechanism is still unknown. Using in situ high resolution transmission electron

microscopy (HR-TEM), we capture the phase transformation-based crystallization process and its kinetics at the sub-nanoscale for the first time, which reveals the anisotropic epitaxial growth and furthermore, explains the orientation control by a combination of molecular dynamic (MD) simulations. The finding provides a more comprehensive and in-depth understanding about crystallization orientation controls.

The spherical ACP nanoparticles and HAP nanorods are synthesized in our laboratory according to the literatures,[33] as demonstrated by their characterizations (Figure S1 and S2). As a control, we examine the phase transformation process of individual ACP adsorbed on carbon film (Figure S3a) and the result shows that multiple crystallization sites appear on both the surface and bulk of an ACP particle. In combination with selected area electron diffraction (SAED), HR-TEM and fast Fourier transformation (FFT) analyses, it is confirmed that these resulting crystals are polycrystalline HAP (Figure S3b-d) and their crystallographic directions are random. It follows that in the control experiment, there is no orientation control in the case of crystallizations from ACP without a HAP substrate, which agrees with the previous understanding.[39]

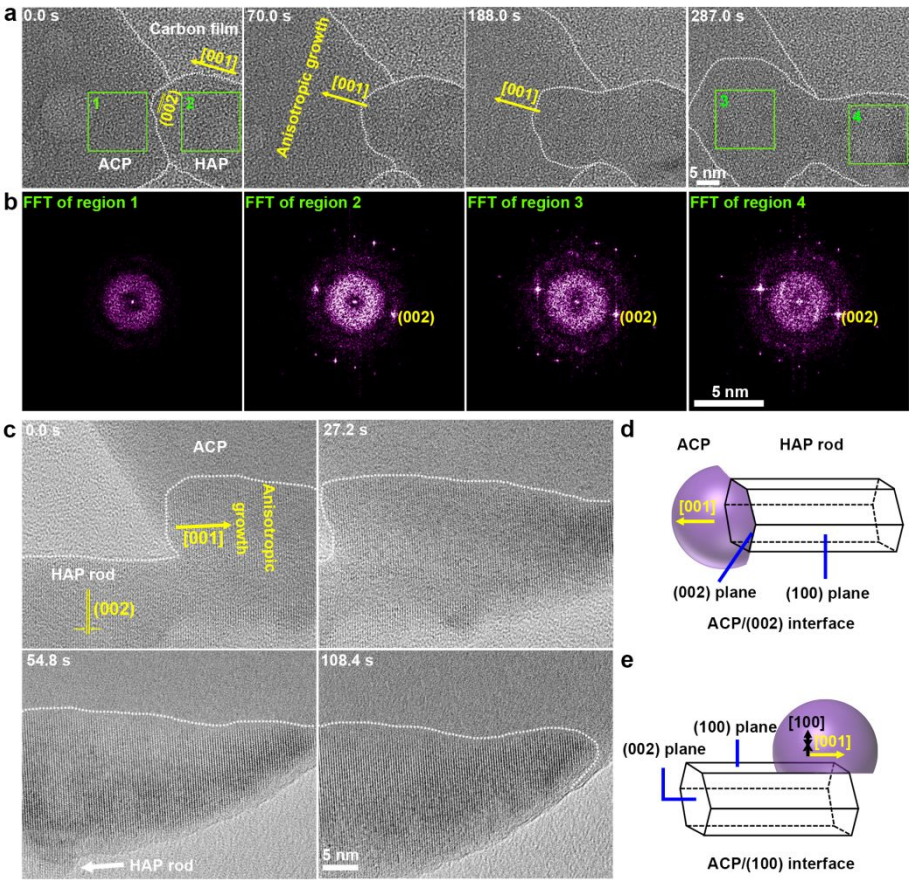

Figure 1. The phase transformation process of ACP to HAP where one HAP nanorod contacts with spherical ACP nanoparticle. (a) In situ TEM image sequences showing the epitaxial growth of HAP along [001] direction marked by yellow arrows. The ACP/HAP/carbon film interface is delineated by white dashed line. (b) The FFT images of different regions highlighted by green frames in a. The corresponding FFT images of region 1, 2, 3 and 4 represent the ACP structure, the original HAP nanorod and newly formed HAP crystal within ACP and final nanorod, respectively. (c) In situ TEM image sequences showing the anisotropic growth of HAP preferentially along [001] direction when ACP contacts with the (100) face of HAP. (d-e) The schemes of contacting form between ACP and HAP, which corresponds to the case in a and c, respectively.

However, this phase transformation process is different in a skillfully designed model system, in which spherical ACP nanoparticles closely contact with HAP nanorod substrate. It is

comparable to the configuration where continuous ACP mineral layer is found at the biomineralization front of delicate mineral structures.[19] As shown in Figure 1a, a series of HR-TEM images display the phase transformation process of ACP to HAP when HAP nanorod contacts with ACP. The HR-TEM (at 0.0 s in Figure 1a) and corresponding FFT images (Figure 1b) of region 1 confirm a typical characteristic of ACP, whereas (002) face lattice fringe and FFT image of region 2 demonstrate the existence of crystalline HAP. The ACP-HAP interface is marked by white dashed lines, which seems to be a continuous structure. It is probably because that ACP particles and HAP rods attach together to achieve closed contact and even fuse into a continuous and homogeneous interfacial structure during the drying process. Notably, the crystallization of ACP to HAP begins from the interface since the interface-induced ordering decays exponentially with distance from the interface,[40] which supports our observations where the region far from the interface keep their original amorphous state. In addition, the newly formed structure is composed of (002) faces, showing a perfect epitaxial matching with the original HAP structure. Such well-ordered and oriented structure at the interface indicates that ACP mediated phase transformation proceeds via the epitaxial growth of HAP along *c*-axis in essence. At 287.0 s, the lattice between newly formed structure and original HAP is exactly same, which can be validated by the identical orientation of region 3 and 4 (Figure 1b). Although the lateral growth can be observed between 188.0 s and 287.0 s, it should be noted that crystallization of HAP proceeds from the tip of rods ([001] direction) with faster growth rates relative to the lateral growth ([100] direction).

Generally, the growth along *c*-axis is advantageous during ACP mediated HAP formation process, regardless of the contacting facets of HAP substrates. For example, despite that ACP initially contacts with the (100) faces of HAP nanorod, only the area closing to the edge of

spherical ACP crystallizes into crystals along *c*-axis (Figure 1c). It is found that the newly generated structure consists of (002) rather than (100) faces, which implies that anisotropic epitaxial crystallization is independent on the HAP substrate. As described by the scheme of position of ACP contacting with HAP (Figure 1d-e), the epitaxial growth along *c*-axis is available, while the growth of *a*- or *b-axis* is disadvantageous even on (100) substrates. By quantifying the growth difference along different orientations, it shows that the aspect ratio (the length along *c*- to the width along *a- or b*- orientation) of newly produced crystal is 2.1±0.3. Assuming constant growth rates during the whole phase transformation process, it indicates that the growth rate along *c-axis* is about two times of those along *a*- and *b*-axis. Clearly, the ACP mediated HAP crystallization occurs via an anisotropic epitaxial growth.

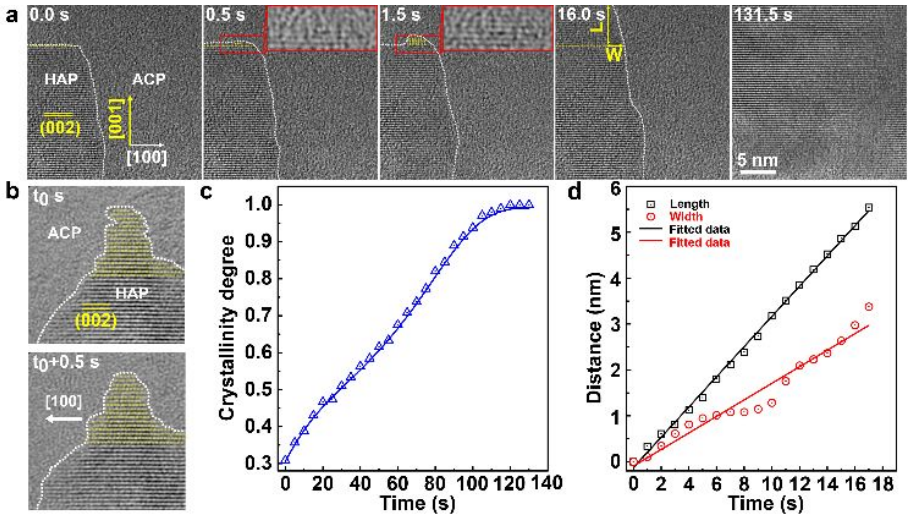

Figure 2. The evolution dynamics of ACP/HAP interface. (a) In situ HR-TEM image sequences showing the detailed crystallization process of HAP from ACP. The growth directions along [001] and [100] are marked. The ACP/HAP interface is separated by dashed white lines. The "L" and "W" represent the length and width direction respectively. (b) The crystallinity degree changes during the phase transformation process. (c) The length and width change with time, showing the preferential epitaxial growth along [001] direction. (d) The lateral epitaxial growth of HAP along [100].

In order to understand how the epitaxial growth preferentially occurs along the *c-axis* orientation, we carefully investigate the evolution dynamics of the growth front which corresponds to the ACP-HAP-(002) face interface (Figure 2a). Initially, a continuous ACP-HAP interface is visible. Subsequently, a new layer forms from the last (002) face at 0.5 s, which is highlighted by the yellow dashed lines. At 1.5 s, two new layers produce on the just-formed layer. The newly formed layer is perpendicular to *c*-axis orientation with highly ordered structure where the epitaxial growth of HAP begins on the inner (002) face. Notably, the laterally epitaxial growth of HAP along *a*- or *b*- orientation advances simultaneously (Figure 2b), which grows from side face of newly formed (002) layers. In addition, the crystallinity of ACP (defined as the ratio of projected area between amorphous and crystalline part) increases linearly to 1.0 (Figure

2c). It indicates the rate of phase transformation is constant. The ACP can completely transform into HAP via epitaxial and lateral growth. Likewise, the growth rate of HAP from along different directions is investigated (Figure 2d). The growth rate along *c*-axis is ~ 0.35 nm/s, which roughly corresponds to one (002) layer/second. Whereas it corresponds to ~ 0.18 nm/s along *a*- or *b*-axis orientation, confirming the anisotropic behavior quantitatively.

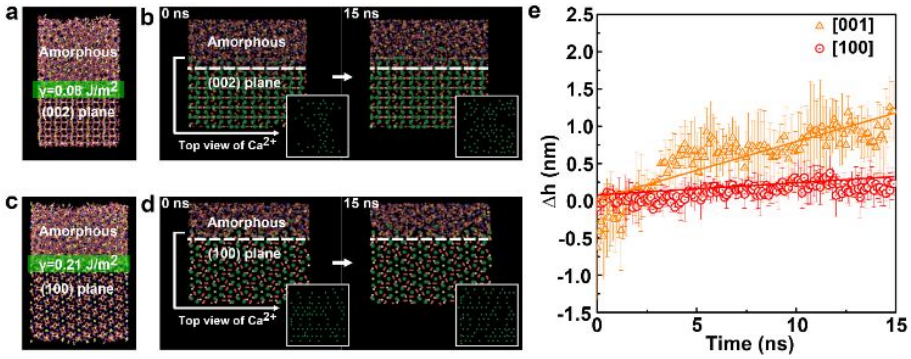

Figure 3. The molecular dynamics simulations. (a, c) Interfacial energies of ACP-HAP-(002) face and ACP-HAP-(100) face, respectively. (b, d) Growth of HAP on (001) and (100) substrate, with a top view showing the Ca^{2+} grown upon the interface. (e) The height of the new grown HAP (Δh) is plotted as a function of time t, using data from three independent MD simulations for [100] and [001] growth respectively.

Previous works have emphasized the importance of interfacial energies in crystal growth.[41,42] For example, negative HAP-(001)-water and positive HAP-(100)-water interfacial energies provide a reasonable explanation for the empirical observation of the relatively small surface area of the (002) face in inorganically grown HAP crystal.[43] And thus we suggest that the activation energy barrier for phase transformation may rely on the interfacial energy of ACP-HAP interface. To elucidate the role of different interfaces in anisotropic epitaxial growth of HAP, we employed classical atomistic models to calculate the interfacial energies of ACP-HAP-(002) and ACP-HAP-(100) face, respectively (Table S1, more technical details can be found in

the Supporting Information). Results show that interfacial energy follows the order of $\gamma_{ACP\text{-}HAP\text{-}(002)}$ (0.08 J/m^2) < $\gamma_{ACP\text{-}HAP\text{-}(100)}$ (0.21 J/m^2). We suggest that the lower interfacial energy of ACP-HAP-(002) interface is probably due to the intrinsic crystalline features of HAP, which stems from its special structure of (002) face. Specifically, it is believed that the (002) face of HAP includes hexagonal packing of Posner's clusters ($Ca_9(PO_4)_6$), and these clusters also appear within ACP structure.[44,45] As described in the cluster growth model during HAP growth process,[45] the phase transformation involves an epitaxial matching between ACP and HAP substrate, where local rearrangement process of attacked $Ca_9(PO_4)_6$ clusters occurs. It should be noted that the interfacial energy reflects the intermolecular interactions between HAP and closely contacted ACP, which possibly contribute to spontaneous structural rearrangement of clusters.[18] The lower interfacial energy of ACP-HAP-(002) means less structural mismatch between ACP and HAP-(002). It might be interpreted as a lower activation energy barrier (E) required for direct structural rearrangement of clusters at the ACP-HAP-(002) interface. Consequently, the growth of (002) faces is preferred and then, a following question is how the activation energy barrier controls the transformation from ACP to HAP at nanoscale.

It is speculated that the rate-limiting process of HAP growth is the incorporation of clusters during ACP mediated HAP crystallization process.[44] To quantitatively estimate the resistance of phase transformation process, the kinetic coefficient is introduced. During the growth process of HAP, the rate is described by the following equation:[44]

$$v = \beta C_e \omega \sigma \qquad (1)$$

where V is growth velocity, β, kinetic coefficient, C_e, saturated concentration of HAP, ω, the molecular weight of crystal, and σ, degree of supersaturation. The item of β can be expressed as:

$$\beta = Aexp(-E/KT) \qquad (2)$$

where, *E* represents the activation energy required for the incorporation of clusters, *T*, the system temperature, and *k,* the Molar gas constant. From these two equations, we can qualitatively explain the anisotropic epitaxial growth of HAP from the view of activation energy barrier: the lower E of clusters rearrangement at ACP-HAP-(002) interface dedicates higher growth rate of HAP and then drives the preferential HAP growth along *c*-axis. In brief, continuous epitaxial growth promotes the anisotropic phase transformation of ACP to HAP. As demonstrated by MD simulation results via building different ACP-HAP interfaces (Figure S4, Figure 3b and d, more technical details can be found in the Supporting Information), it is found that the growth rate along *c-axis* is obviously faster than the one along *a*- or *b-axis* (Figure 3e and Table S2). Such trend is comparable to our experimental observations where growth rate along [001] direction is almost twice the one along [100] direction (Figure 2c).

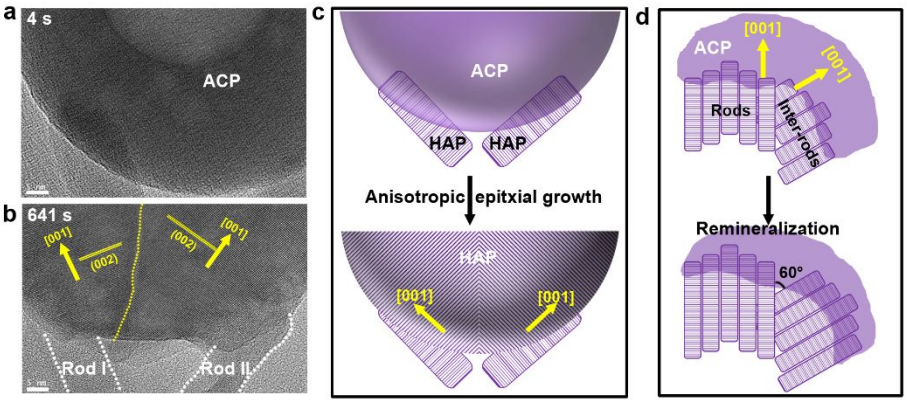

Figure 4. The phase transformation of ACP based on HAP nanorod with different directions. (a, b) In situ TEM image sequences showing the phase transformation process of ACP to HAP where two HAP nanorods contact with spherical ACP nanoparticle. Scale bar, 5 nm. (c) The scheme of phase transformation process in a and b. (d) The scheme of enamel re-mineralization process with preferential *c-axis* growth.

This finding can provide an understanding about crystallographic orientation controls in biomineralization with structural complexity. During biological formation of hard tissues, the biomineralization frontier is the integrated crystalline-amorphous interface.[19,25,46] It is interesting

and important that the microstructures and orientations of the newly generated crystals can be strictly duplicated during the amorphous phase mediated crystallization process in nature.[46] For example, the growth of HAP rods with tightly packed and well-defined orientations is the key to ensuring the high mechanical strength of dental enamel.[10,33] Notably, this anisotropic epitaxial growth along *c-axis* is related to the initial direction of HAP rods, which can be associated with our recent achievement of enamel repair.[33] It shows that a rational designed ACP layer on enamel can transform into the well-ordered HAP with the exactly same structure of natural enamel by mimicking the biomineralization frontier. In Figure 4a, two HAP nanorods with different directions closely contact with ACP, giving rise to the appearance of two ACP-HAP-(002) interfaces. The ACP gradually transforms into crystalline materials by preferential *c-axis* crystallization along original HAP rods (Figure S5), which are identified as HAP from lattice fringe spacing of (002) faces (Figure 4b) and corresponding SAED image (Figure S6). Meanwhile, it should be stressed that the epitaxial direction of newly grown HAP is different from each other, which depends on the direction of HAP substrates (Figure 4c). Accordingly, although both enamel prisms and inter-prisms are HAP, there is an angle of approximately 60° between them to produce the characteristic "honeycomb" appearance.[9] It is the structure configuration that makes enamel possess more remarkable microtribiological behavior than artificial HAP rods.[47] Therefore, the finding of anisotropic epitaxial growth provides a reasonable explanation at the nanoscale why and how ACP can evolve into well-aligned HAP rods along enamel prisms and inter-prisms direction during the re-mineralization process of enamel (Figure 4d).

In summary, the direct experimental observations of ACP mediated HAP crystallization process and corresponding MD simulations provide an alternative understanding about the

general *c-axis* orientation control of HAP. Our research proves that the existence of amorphous-crystalline interface can initiate the oriented crystallization, and notably in the absence of any organic additives or matrixes, which is different from previous understanding on biomineralization that the formation of well-aligned biological minerals needs organic macromolecules or matrixes. Furthermore, this work suggests that the anisotropic epitaxial growth plays a key role in the simultaneous controls of building complex biomaterials with highly-ordered structure and multi- growth orientations, opening an alternative way to construct biomimetic functional materials with rational designed orientation.

ASSOCIATED CONTENT

Supporting Information.

The following files are available free of charge on the ACS Publications website at DOI: 10.1021/acs.jpclett.

Details for the TEM sample preparations, experimental methods for analyses and theoretical methodologies, Figures S1−S7 and Table S1-S2. (PDF)

In situ TEM movies showing the detailed crystallization process of ACP to HAP. (AVI)

AUTHOR INFORMATION

Corresponding Author

*oldliu@zju.edu.cn

*rtang@zju.edu.cn

Author Contributions

B.J. and R.T. designed the project. B.J., C.S., Z.L. and Z.M. conducted the experiments. B.J., C.S., Z.L. and R.T. analyzed the data. Y.M. performed the molecular dynamic simulations. The manuscript was written with contributions of all authors. All authors have given approval to the final version of the manuscript.

Notes

The authors declare no competing financial interests.

ACKNOWLEDGMENT

This work was financially supported by the National Natural Science Foundation of China (21625105 and 21805241). The experiments of electron microscopy were performed at the Center of Electron Microscopy of Zhejiang University. We thank Dr. Chuanhong Jin for technical supports. The computation resource was provided by National Energy Research Scientific Computing Center of US (NERSC).

REFERENCES

(1) Holmes, J. D.; Johnston, K. P.; Doty, R. C.; Korgel, B. A. Control of Thickness and Orientation of Solution-Grown Silicon Nanowires. *Science* **2000**, *287*, 1471-1473.

(2) Yoon, Y.; Park, C.; Kim, J.; Shin, D. Lattice Orientation Control of Lithium Cobalt Oxide Cathode Film for All-Solid-State Thin Film Batteries. *J. Power Sources* **2013**, *226*, 186-190.

(3) Kuykendall, T. R.; Altoe, M. V. P.; Ogletree, D. F.; Aloni, S. Catalyst-Directed Crystallographic Orientation Control of GaN Nanowire Growth. *Nano Lett.* **2014**, *14*, 6767-6773.

(4) Okaniwa, M.; Oaki, Y.; Kaneko, S.; Ishida, K.; Maki, H.; Imai, H. Advanced Biomimetic Approach for Crystal Growth in Nonaqueous Media: Morphology and Orientation Control of Pentacosadiynoic Acid and Applications. *Chem. Mater.* **2015**, *27*, 2627-2632.

(5) Ma, X. Y.; Li, Y. Y.; Wang, C. W.; Sun, Y.; Ma, Y. F.; Dong, X. L.; Qian, J. C.; Yuan, Y.; Liu, C. S. Controlled Synthesis and Transformation of Nano-Hydroxyapatite with Tailored Morphologies for Biomedical Applications. *J. Mater. Chem. B* **2017**, *5*, 9148-9156.

(6) Han, H. S.; Shin, S.; Kim, D. H.; Park, I. J.; Kim, J. S.; Huang, P. S.; Lee, J. K.; Cho, I. S.; Zheng, X. L. Boosting the Solar Water Oxidation Performance of A $BiVO_4$ Photoanode by Crystallographic Orientation Control. *Energy Environ. Sci.* **2018**, *11*, 1299-1306.

(7) Wang, W.; Oaki, Y.; Ohtsuki, C.; Nakano, T.; Imai, H. Formation of c-axis-Oriented Columnar Structures through Controlled Epitaxial Growth of Hydroxyapatite. *J. Asian Ceramic Soc.* **2018**, *1*, 143-148.

(8) Liu, L.; Sushko, M. L.; Buck, E. C.; Zhang, X.; Kovarik, L.; Shen, Z.; Tao, J.; Nakouzi, E.; Liu, J.; De Yoreo, J. J. Revisiting the Growth Mechanism of Hierarchical Semiconductor Nanostructures: The Role of Secondary Nucleation in Branch Formation. *J. Phys. Chem. Lett.* **2019**, *10*, 6827-6834.

(9) White, S.; Luo, W.; Paine, M.; Fong, H.; Sarikaya, M.; Snead, M. Biological Organization of Hydroxyapatite Crystallites into A Fibrous Continuum Toughens and Controls Anisotropy in Human Enamel. *J. Dent. Res.* **2001**, *80*, 321-326.

(10) Fratzl, P.; Weinkamer, R. Nature's Hierarchical Materials. *Prog. Mater Sci.* **2007**, *52*, 1263-1334.

(11) Radha, B.; Kulkarni, G. U. A Modified Micromolding Method for Sub-100-nm Direct Patterning of Pd Nanowires. *Small* **2009**, *5*, 2271-2275.

(12) Yang, H. J.; He, S. Y.; Tuan, H. Y. Self-seeded Growth of Five-Fold Twinned Copper Nanowires: Mechanistic Study, Characterization, and SERS Applications. *Langmuir* **2014**, *30*, 602-610.

(13) Meena, S. K.; Sulpizi, M. From Gold Nanoseeds to Nanorods: The Microscopic Origin of the Anisotropic Growth. *Angew. Chem. Int. Edit.* **2016**, *55*, 11960-11964.

(14) Jackson, S. R.; McBride, J. R.; Rosenthal, S. J.; Wright, D. W. Where's the Silver? Imaging Trace Silver Coverage on the Surface of Gold Nanorods. *J. Am. Chem. Soc.* **2014**, *136*, 5261-5263.

(15) Nielsen, M. H.; Aloni, S.; De Yoreo, J. J. In Situ TEM Imaging of $CaCO_3$ Nucleation Reveals Coexistence of Direct and Indirect Pathways. *Science* **2014**, *345*, 1158-1162.

(16) Jiang, S.; Pan, H.; Chen, Y.; Xu, X.; Tang, R. Amorphous Calcium Phosphate Phase-Mediated Crystal Nucleation Kinetics and Pathway. *Faraday Discuss.* **2015**, *179*, 451-461.

(17) Rodriguez-Navarro, C.; Burgos Cara, A.; Elert, K.; Putnis, C. V.; Ruiz-Agudo, E. Direct Nanoscale Imaging Reveals the Growth of Calcite Crystals via Amorphous Nanoparticles. *Cryst. Growth Des.* **2016**, *16*, 1850-1860.

(18) Tsuji, T.; Onuma, K.; Yamamoto, A.; Iijima, M.; Shiba, K. Direct Transformation from Amorphous to Crystalline Calcium Phosphate Facilitated by Motif-Programmed Artificial Proteins. *Proc. Natl. Acad. Sci. U.S.A.* **2008**, *105*, 16866-16870.

(19) Mahamid, J.; Aichmayer, B.; Shimoni, E.; Ziblat, R.; Li, C.; Siegel, S.; Paris, O.; Fratzl, P.; Weiner, S.; Addadi, L. Mapping Amorphous Calcium Phosphate Transformation into Crystalline Mineral from the Cell to the Bone in Zebrafish Fin Rays. *Proc. Natl. Acad. Sci. U.S.A.* **2010**, *107*, 6316-6321.

(20) Rodríguez-Navarro, A. B.; Marie, P.; Nys, Y.; Hincke, M. T.; Gautron, J. Amorphous Calcium Carbonate Controls Avian Eggshell Mineralization: A New Paradigm For Understanding Rapid Eggshell Calcification. *J. Struct. Biol.* **2015**, *190*, 291-303.

(21) Mass, T.; Giuffre, A. J.; Sun, C.-Y.; Stifler, C. A.; Frazier, M. J.; Neder, M.; Tamura, N.; Stan, C. V.; Marcus, M. A.; Gilbert, P. U. Amorphous Calcium Carbonate Particles Form Coral Skeletons. *Proc. Natl. Acad. Sci. U.S.A.* **2017**, *114*, E7670-E7678.

(22) Su, J.; Zhu, F.; Zhang, G.; Wang, H.; Xie, L.; Zhang, R. Transformation of Amorphous Calcium Carbonate Nanoparticles into Aragonite Controlled by ACCBP. *CrystEngComm* **2016**, *18*, 2125-2134.

(23) Brès, E.; Voegel, J. C.; Frank, R. High-Resolution Electron Microscopy of Human Enamel Crystals. *J. Microsc.* **1990**, *160*, 183-201.

(24) Jeong, N.; Cha, M.; Park, Y. C.; Lee, K. M.; Lee, J. H.; Park, B. C.; Lee, J. Single-Crystal Apatite Nanowires Sheathed in Graphitic Shells: Synthesis, Characterization, and Application. *ACS Nano* **2013**, *7*, 5711-5723.

(25) La Fontaine, A.; Zavgorodniy, A.; Liu, H.; Zheng, R.; Swain, M.; Cairney, J. Atomic-Scale Compositional Mapping Reveals Mg-Rich Amorphous Calcium Phosphate in Human Dental Enamel. *Sci. Adv.* **2016**, *2*, e1601145.

(26) Reznikov, N.; Bilton, M.; Lari, L.; Stevens, M. M.; Kroger, R. Fractal-Like Hierarchical Organization of Bone Begins at the Nanoscale. *Science* **2018**, *360*.

(27) Iijima, M.; Onuma, K. Roles of Fluoride on Octacalcium Phosphate and Apatite Formation on Amorphous Calcium Phosphate Substrate. *Cryst. Growth Des.* **2018**, *18*, 2279-2288.

(28) Xu, Z.; Yang, Y.; Wang, Z.; Mkhonto, D.; Shang, C.; Liu, Z. P.; Cui, Q.; Sahai, N. Small Molecule-Mediated Control of Hydroxyapatite Growth: Free Energy Calculations Benchmarked to Density Functional Theory. *J. Comput. Chem.* **2014**, *35*, 70-81.

(29) Wang, H.; Xiao, Z.; Yang, J.; Lu, D.; Kishen, A.; Li, Y.; Chen, Z.; Que, K.; Zhang, Q.; Deng, X.; Yang, X.; Cai, Q.; Chen, N.; Cong, C.; Guan, B.; Li, T.; Zhang, X. Oriented and Ordered Biomimetic Remineralization of the Surface of Demineralized Dental Enamel Using HAP@ACP Nanoparticles Guided by Glycine. *Sci. Rep.* **2017**, *7*, 40701.

(30) Wang, X.; Zhuang, J.; Peng, Q.; Li, Y. D. Liquid–Solid–Solution Synthesis of Biomedical Hydroxyapatite Nanorods. *Adv. Mater.* **2006**, *18*, 2031-2034.

(31) Chen, J. D.; Wang, Y. J.; Wei, K.; Zhang, S. H.; Shi, X. T. Self-Organization of Hydroxyapatite Nanorods through Oriented Attachment. *Biomaterials* **2007**, *28*, 2275-2280.

(32) Costa, D. O.; Dixon, S. J.; Rizkalla, A. S. One- and Three-Dimensional Growth of Hydroxyapatite Nanowires During Sol-Gel-Hydrothermal Synthesis. *ACS Appl. Mater. & Interf.* **2012**, *4*, 1490-1499.

(33) Shao, C. Y.; Jin, B.; Mu, Z.; Lu, H.; Zhao, Y. Q.; Wu, Z. F.; Yan, L. M.; Zhang, Z. S.; Zhou, Y.; Pan, H. H.; Liu, Z. M.; Tang, R. K. Repair of Tooth Enamel by A Biomimetic Mineralization Frontier Ensuring Epitaxial Growth. *Sci. Adv.* **2019**, *5*, eaaw9569.

(34) Narayan, J. Interface Structures during Solid-Phase-Epitaxial Growth in Ion Implanted Semiconductors and A Crystallization Model. *J. Appl. Phys.* **1982**, *53*, 8607-8614.

(35) Garnett, E. C.; Liang, W.; Yang, P. Growth and Electrical Characteristics of Platinum-Nanoparticle-Catalyzed Silicon Nanowires. *Adv. Mater.* **2007**, *19*, 2946-2950.

(36) Chou, Y. C.; Wu, W. W.; Cheng, S. L.; Yoo, B. Y.; Myung, N.; Chen, L. J.; Tu, K. In-Situ TEM Observation of Repeating Events of Nucleation in Epitaxial Growth of Nano $CoSi_2$ in Nanowires of Si. *Nano Lett.* **2008**, *8*, 2194-2199.

(37) Song, M.; Lee, J.; Wang, B.; Legg, B. A.; Hu, S.; Chun, J.; Li, D. In Situ Characterization of Kinetics and Mass Transport of PbSe Nanowire Growth via LS and VLS Mechanisms. *Nanoscale* **2019**, *11*, 5874-5878.

(38) Bogicevic, A.; Strömquist, J.; Lundqvist, B. I. Low-Symmetry Diffusion Barriers in Homoepitaxial Growth of Al (111). *Phys. Rev. Lett.* **1998**, *81*, 637.

(39) Wang, C. G.; Liao, J. W.; Gou, B. D.; Huang, J.; Tang, R. K.; Tao, J. H.; Zhang, T. L.; Wang, K. Crystallization at Multiple Sites Inside Particles of Amorphous Calcium Phosphate. *Cryst. Growth Des.* **2009**, *9*, 2620-2626.

(40) Oh, S. H.; Chisholm, M. F.; Kauffmann, Y.; Kaplan, W. D.; Luo, W.; Rühle, M.; Scheu, C. Oscillatory Mass Transport in Vapor-Liquid-Solid Growth of Sapphire Nanowires. *Science* **2010**, *330*, 489-493.

(41) Tang, R.; Darragh, M.; Orme, C. A.; Guan, X.; Hoyer, J. R.; Nancollas, G. H. Control of Biomineralization Dynamics by Interfacial Energies. *Angew. Chem. Int. Edit.* **2005**, *44*, 3698-3702.

(42) Hu, Y.; Neil, C.; Lee, B.; Jun, Y. S. Control of Heterogeneous Fe(III) (Hydr)oxide Nucleation and Growth by Interfacial Energies and Local Saturations. *Environ. Sci. Technol.* **2013**, *47*, 9198-9206.

(43) Zhao, W.; Xu, Z.; Yang, Y.; Sahai, N. Surface Energetics of the Hydroxyapatite Nanocrystal-Water Interface: A Molecular Dynamics Study. *Langmuir* **2014**, *30*, 13283-13292.

(44) Onuma, K. Recent Research on Pseudobiological Hydroxyapatite Crystal Growth and Phase Transition Mechanisms. *Prog. Cryst. Growth Charact. Mater.* **2006**, *52*, 223-245.

(45) Onuma, K.; Ito, A. Cluster Growth Model for Hydroxyapatite. *Chem. Mater.* **1998**, *10*, 3346-3351.

(46) Nassif, N.; Pinna, N.; Gehrke, N.; Antonietti, M.; Jäger, C.; Cölfen, H. Amorphous Layer around Aragonite Platelets in Nacre. *Proc. Natl. Acad. Sci. U.S.A.* **2005**, *102*, 12653-12655.

(47) Zheng, J.; Li. Y.; Shi, M. Y.; Zhang, Y. F.; Qian, L. M.; Zhou, Z. R. Microtribological Behaviour of Human Tooth Enamel and Artificial Hydroxyapatite. *Tribol. Intern.* **2013**, *63*, 177-185.